Relaxation of spheromak configurations with open flux

Pablo Luis García-Martínez[1,*] and Ricardo Farengo[1]

[1]*Centro Atómico Bariloche (CNEA) and Instituto Balseiro (UNC-CNEA) San Carlos de Bariloche, RN 8400, Argentina*

Abstract

The relaxation of several kink unstable equilibria with open flux representative of spheromaks sustained by dc helicity injection, is studied by means of three-dimensional, resistive magnetohydrodynamic (MHD) simulations. No external driving is applied, but the initial conditions are chosen to reproduce the current profiles existing in a gun driven spheromak, which has a high current density in the open flux region and a low current density in the closed flux region. The growth and non linear saturation of various unstable modes, the dynamo action which converts toroidal flux into poloidal flux and the evolution of the λ profile ($\lambda = \mu_0 \mathbf{J} \cdot \mathbf{B}/B^2$) are studied. An initial condition is found which results in a dynamo that produces enough poloidal flux to compensate the resistive losses occured during a characteristic time of the instability. The flux amplification factor around which this case oscillates is consistent with existing experimental data. During the relaxation, the central open flux tube develops a helical distortion and the closed flux surfaces are destroyed. After the relaxation event, close flux surfaces form again but the final profiles are not fully relaxed and the central open flux tube remains distorted. The effect of the Lundquist number on the evolution and its impact on the required level of fluctuations are evaluated. Finally, the dynamics of the system for different current levels in the open flux region is studied.

*pablogm@cab.cnea.gov.ar

I. INTRODUCTION

Steady state current drive by means of helicity injection with dc electrodes [1, 2] is an attractive sustainment method that has been used [3–6] or proposed [7] in several experiments involving spheromaks and spherical tokamaks. This method relies on the relaxation of the magnetic configuration, which is driven unstable by the voltage applied across the open flux region. Relaxation theory predicts the required redistribution of currents [8], but it gives no details about the physical mechanism and the dynamics of the system during the current redistribution. In agreement with the theoretical predictions [9], experiments indicate that fluctuations with toroidal mode number $n = 1$ are ubiquitous in helicity-injected spheromaks and play a central role in the process by which current is transferred from the driven central open flux region (the "column") to the closed flux region (the "annulus") [10]. It has been observed that the $n = 1$ fluctuations produce a helical structure, presumably arising from the finite amplitude saturation of a kink instability, which rotates and has a strongly asymmetric return ("return column") around the annulus [11].

Ideal linear stability analysis of equilibria relevant to helicity injected spheromaks have been carried out, including both open and closed flux and realistic current profiles [12]. The results from Ref. [12] show that the configuration becomes kink unstable when the open flux current density is increased. It is expected that driven configurations would operate near the stability boundary for this mode. However, relevant questions like how unstable the configuration should become in order to produce the required current redistribution (which occurs during the non-linear phase of the instability), or which is the level of fluctuations associated to that current redistribution, are beyond the scope of linear stability analysis. In this paper, we address these and other questions using numerical simulations.

Numerical simulations have been used to study spheromak dynamics in the past. Katayama and Katsurai [13] computed the evolution of decaying spheromaks with several q profiles in a cylindrical flux conserver without open flux. Formation and sustainment in both a cylindrical "flux core" and a coaxial gun geometries were studied by Sovinec et al [14]. They incorporated electrostatic driving in nonlinear MHD simulations by applying an axial current along an artificial layer of high resistivity at the flux conserver walls. The evolution of an unstable spheromak equilibrium in a "bowtie" flux conserver, without open flux, was simulated by Izzo and Jarboe [15]. Using a fixed initial condition, having a linear

$\lambda(\psi)$ profile (where $\lambda = \mu_0 \mathbf{J} \cdot \mathbf{B}/B^2$, and ψ is the poloidal flux), they varied the Lundquist number, S, over one order of magnitude and identified a minimum value for flux generation. More recently [16], the evolution of spheromak equilibria inside a cylindrical flux conserver with different initial λ profiles and different S, was studied. While very unstable configurations were observed to fully relax toward the Taylor state, marginally unstable cases showed only partially relaxed final profiles. Furthermore, it was found that increasing S led to a higher level of fluctuations and poloidal flux generation but, despite the stronger activity, the final level of relaxation was determined only by the initial condition (in the high S regime considered there).

In this work, we present the first non-linear MHD simulations of configurations having initial $\lambda(\psi)$ profiles represented by a tanh function, which were used to fit experimental data from SPHEX [10]. Our computations also incorporate an open flux region linking a pair of concentric electrodes at one end of a cylindrical flux conserver, and can be regarded as a complete study of the non-linear phase of the linear instabilities considered in Ref. [12]. The evolution of these configurations is computed for the time scale of the kink instability, which is much smaller than the resistive time scale (high Lundquist number regime). This study is focused on the relaxation process that converts the poloidal current in the open flux region into toroidal current in the surrounding closed flux region, leaving aside (for the moment) the mechanism by which the current in the open flux is forced.

The stability of the configurations studied here is determined by the $\lambda(\psi)$ profile, which is characterized (Sec. II) by its values in the column (λ_c) and in the annulus (λ_a). In agreement with previous studies [12], our results show that, for a fixed λ_c, the kink instability becomes stronger (i.e. it has a larger growth rate) when λ_a is decreased. When the instability is strong enough, the relaxation of the configuration brings about the desired effect of flux conversion, from toroidal to poloidal. We identify a threshold value for λ_a, above which the instability is too weak to compensate the resistive decay of the poloidal flux during the typical time of the instability (Sec. III D). This threshold lies in the unstable region of the linear stability map presented in Ref. [12]. We show that, when the evolution near this threshold is considered, the flux amplification factor ($A_\psi = \psi_{ma}/\psi_G$, where ψ_{ma} and ψ_G are the poloidal fluxes at the magnetic axis and at the gun, respectively) around which the system oscillates is consistent with experimental observations (for the λ_c and S employed). This case is considered as the most representative of a spheromak in the sustainment phase and is studied in detail.

In Sec. III A several global quantities, including the fluctuation spectrum, and radial profiles are shown. The comparison of the final profiles with the fully relaxed uniform λ state clearly shows that the final configuration is only partially relaxed. The magnetic flux surfaces during this relaxation event are analyzed in Sec. III B. Upon instability saturation, the central column exhibits a helical distortion and a return column which concentrates the return flux. This structure is similar to that observed experimentally by Duck et al. [11] and, up to our knowledge, has not been reproduced by numerical simulations before. In Sec. III C the component of the dynamo electric field parallel to the magnetic field is studied. The effect of the Lundquist number on the instability evolution and the level of fluctuations required to maintain A_ψ are discussed in Sec. III E. We also investigate the behavior of the system for different values of λ_c (Sec. III F). Our simulations indicate that when a higher λ_c is imposed, a stronger instability is required to sustain A_ψ against resistive decay. Finally, the conclusions are sumarized in Sec. IV.

II. SIMULATION DESCRIPTION

Using the Versatile Advection Code [17], we solve the isothermal resistive MHD equations employing a finite volume method with a total variation diminishing Roe's approximate Riemann solver. The $\nabla \cdot \mathbf{B} = 0$ condition is maintained using the projection method [18]. To simplify the physics, we do not advance the density. This corresponds to a constant pressure computation, usually referred to as the zero-β (or zero-pressure) approximation, widely used when modeling low-β plasmas [14–16]. The MHD equations are normalized using a length scale R (the flux conserver radius), a density scale ρ_0 and a typical magnetic field magnetic B_0. With these quantities we can define the velocity scale $c_A = B_0/\sqrt{\mu_0 \rho_0}$ (Alfvèn velocity), the time scale $\tau_A = R/c_A$ (Alfvèn time) and the current density scale $J_0 = B_0/\mu_0 R$. The resulting dimensionless equations are

$$\frac{\partial \mathbf{u}}{\partial t} + \mathbf{u} \cdot \nabla \mathbf{u} = \frac{\mathbf{J} \times \mathbf{B}}{\rho_0} + \tilde{\nu} \nabla \cdot \Pi, \tag{1}$$

$$\frac{\partial \mathbf{B}}{\partial t} + \nabla \times \mathbf{E} = 0, \tag{2}$$

where $\mathbf{J} = \nabla \times \mathbf{B}$, $\mathbf{E} = -\mathbf{u} \times \mathbf{B} + \tilde{\eta} \mathbf{J}$ and $\Pi = (\nabla \mathbf{u} + \nabla \mathbf{u}^{\mathrm{T}}) - 2/3(\nabla \cdot \mathbf{u})$. The parameter $\tilde{\nu} = \nu/(Rc_A)$ is the dimensionless kinematic viscosity, and $\tilde{\eta} = \eta/(\mu_0 R c_A)$ is the dimensionless resistivity. Both are spatially uniform. In this work we use $\tilde{\eta} = 2 \times 10^{-5}$ and $P_m = \tilde{\nu}/\tilde{\eta} = 1$, which are high enough to make the numerical dissipation introduced by the numerical grid unimportant [16]. The resistive time scale is taken to be $\tau_r = \mu_0/(\eta\lambda_1^2)$ [15], where λ_1 is the first eigenvalue of the force-free equation $\nabla \times \mathbf{B} = \lambda_n \mathbf{B}$ (for a cylinder with $R = h = 1$, $\lambda_1 = 4.955$). The resulting Lundquist number ($S = \tau_r/\tau_A$) is ~ 2000.

A uniform cartesian grid ($N_x \times N_y \times N_z = 100 \times 100 \times 50$) is used to advance the equations in time and a poloidal grid ($N_r \times N_z = 50 \times 50$) containing the Fourier coefficients of the toroidal decomposition is employed to analyze the results. The geometry considered corresponds to a gun produced spheromak with a cylindrical flux conserver and concentric electrodes at one end. The elongation is one ($R = h = 1$) and the boundary conditions imposed (interpolating from the cartesian grid) at the flux conserver are $\mathbf{B} \cdot \mathbf{n} = 0$, $\mathbf{J} \times \mathbf{n} = 0$ and $\mathbf{u} = 0$ (see Ref. [16] for further details). At the electrode end ($z = 0$) the poloidal flux (constant during all the simulation time) is prescribed (see below). With these boundary conditions there is no energy flux across the boundary of the domain.

The force-free equilibria studied in the simulations are obtained by solving the non-linear Grad-Shafranov equation with λ ($\lambda = \mathbf{J} \cdot \mathbf{B}/B^2$, in dimensionless units) taken as a function of the poloidal flux [10, 12]

$$\lambda(\psi) = \lambda_c + \frac{\lambda_c - \lambda_a}{2}\{\tanh[\delta(1-\psi)] - 1\}, \tag{3}$$

where δ ($\delta = 4$ in this study) controls the stepness of the transition from λ_c (in the column) to λ_a (in the annulus). Figure 1 shows the λ profile and flux contours for a typical equilibrium, with $\lambda_a = 3.6$ and $\lambda_c = 12$. The boundary conditions employed to calculate the equilibria are $\psi = 0$ at the flux conserver walls and $\psi(r, z = 0) = C\psi_G r^2(1-r)^3$ at the electrode end, where $C = 28.935$ is a normalization constant and $\psi_G = 1$ is the flux imposed by the gun (see Appendix B of Ref. [12]). The same condition for the flux at the electrode is applied during the time dependent simulation.

To each initial condition, the corresponding $n = 1$ kink eigenmode is added, rescaled to have 10^{-5} times the energy of the axisymmetric equlibrium. In this way the kink instability is activated immediately at the beginning of the simulation [16].

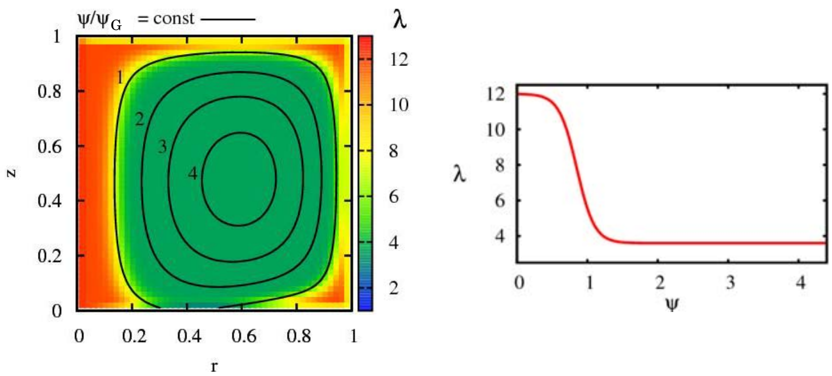

FIG. 1: (Color online) Flux contours and $\lambda(\psi)$ profile for a typical initial condition.

III. RESULTS AND DISCUSSION

In this Section we analyze in detail several aspects of the evolution of the case $\lambda_c = 12$ and $\lambda_a = 3.6$ (Sections III A to III C). Then we present the numerical results obtained when λ_a is varied and λ_c is held constant (Section III D). These results justify why we have chosen the case ($\lambda_c = 12$,$\lambda_a = 3.6$) as the most representative of the actual situation during spheromak sustainment. In Sec. III E we analyze the effect of the Lundquist number on the evolution. Finally, we study the effect of varying λ_c (Section III F).

A. Magnetic relaxation and flux conversion

In Fig. 2, left side (a-d), we show the evolution of the total magnetic energy and the energy in the $n = 0$ mode (a) (normalized to their initial value), the energy content of the $n = 1, 2$ and 3 modes (b) (normalized to the instantaneous $n = 0$ energy), the poloidal flux at the magnetic axis and the toroidal flux (c) (normalized to the flux of the gun) and the ratio between the magnetic energy and the relative helicity of the $n = 0$ mode (defined to be gauge invariant [19]) (d). It is clear that the growth and non linear interaction of the unstable modes trigger a relaxation event that begins around $t \sim 100$ and lasts until $t \sim 170$. This event is characterized by a rapid decay of magnetic energy relative to magnetic helicity (sharp drop in the ratio between the energy and the helicity), an increase in the poloidal flux and a reduction in the toroidal flux (flux conversion). In the right side of Fig 2, panels (e-g), we show the initial and final radial profiles, at $z = 1/2$, of the magnetic field (e), λ (f)

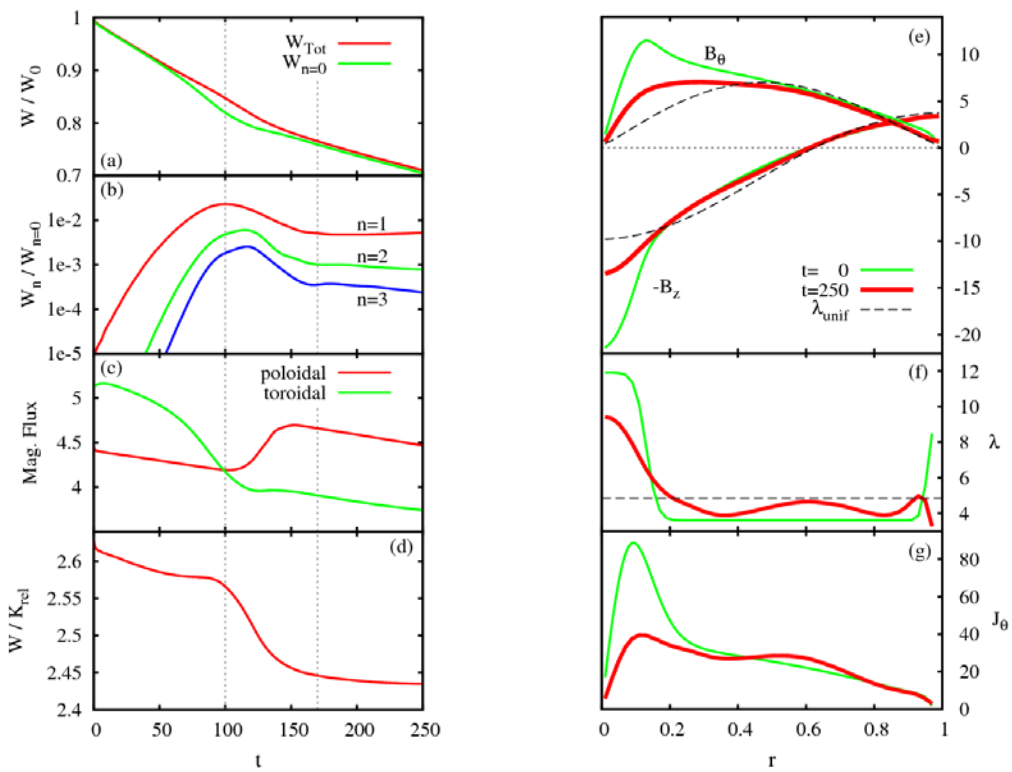

FIG. 2: (Color online) Time evolution of different quantities (a-d) and initial and final radial profiles of the magnetic field (e), λ(f) and the toroidal current density (g).

and the toroidal current density (g) of the $n = 0$ component. The dashed lines in Fig. 2 (e) and (f) correspond to the uniform λ case that has the same relative helicity that the solution at $t = 250$ (with the same boundary condition). It is observed that the final configuration is not in a fully relaxed state. However, this partial relaxation process produces the desired effect of driving a toroidal current in the closed flux region. Note that, despite the resistive decay, the toroidal current density around the magnetic axis increases [$r_{ma} \sim 0.6$, Fig. 2(g)].

B. Magnetic flux surfaces

To visualize the central open flux column, several magnetic field lines (60 lines) are followed from the central electrode (at $r = 0.1$, $z = 0$, and uniformly distributed in the toroidal direction) until they come close to the outer electrode, for three different times. They are shown in Fig. 3. The magnetic lines of the initial column ($t = 0$), return to the

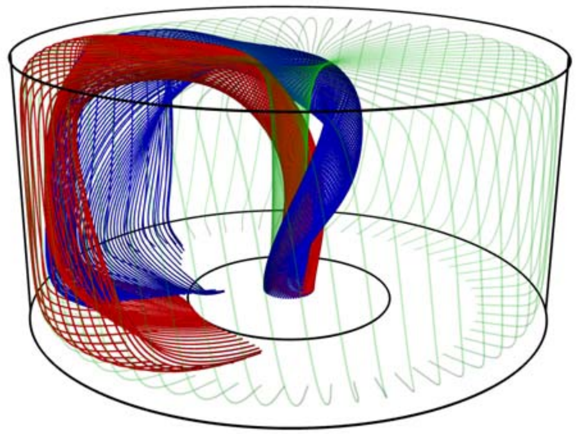

FIG. 3: (Color online) Magnetic field lines beginning at the central electrode, showing the central open flux column at three different times, $t = 0$ (green), $t = 100$ (blue) and $t = 250$ (red), for the $\lambda_c = 12$, $\lambda_a = 3.6$ case.

external concentric electrode axisymmetrically, and they leave the chamber (green lines). At saturation of the kink instability ($t = 100$) the column (blue lines) exhibits a strong helical distortion and its return around the outside of the annulus is strongly asymmetric. A structure of this type has been found experimentally in SPHEX [11].

After the formation of this "return column" most of the lines do not leave the chamber after one single poloidal turn (like at $t = 0$). Instead, they wander through different regions inside the flux conserver at different times (see Figs. 4 and 5). It is worth noting that at the final simulation time ($t = 250$), when the magnetic relaxation event has ceased, the central column (shown in red lines) remains distorted and the return column is still present (at a slightly different toroidal position). This structure is responsible for the persistence of an $n = 1$ component in the energy spectrum during the last 80 Alfvèn times as shown in Fig. 2 (b). The persistence of non-axisymmetric modes after the relaxation has not been observed in previous simulations in closed configurations, even in cases with partially relaxed final states [16, 20].

The fluctuations destroy the closed flux surfaces thus reducing plasma confinement. This is clearly shown in the puncture plots presented in Fig. 4. In these plots, the blue lines begin at the central electrode while the red ones begin at different positions inside the annulus. During the exponential growth of the kink instability ($t = 80$) the closed flux region around

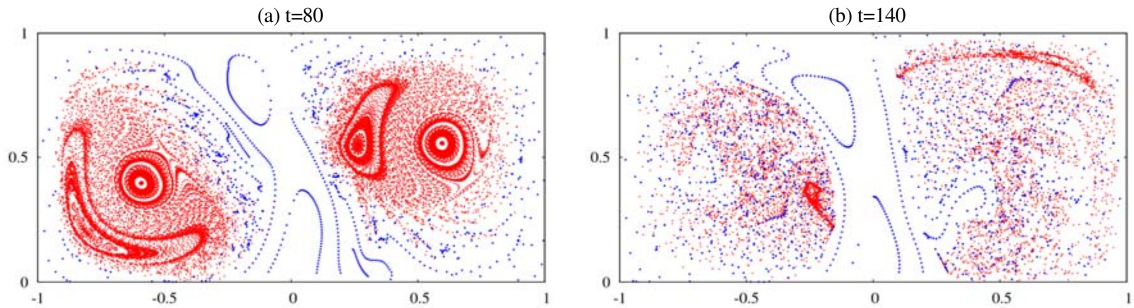

FIG. 4: (Color online) Poincare puncture plots at $t = 80$ and $t = 140$. Blue points correspond to lines beginning at the electrode, and red points, to lines beginning at the annulus.

the magnetic axis shrinks and a magnetic island is formed [Fig. 4(a)]. In Fig. 4 (b), it is observed that at $t = 140$ no closed flux surfaces can be identified. All the lines followed encounter the electrode before travelling a significant distance inside the flux conserver.

After the saturation of the instability and the destruction of the initial closed flux surfaces, the unstable modes decay and closed flux surfaces begin to reappear. In Fig. 5 some magnetic field lines are shown for three different times (upper row), sketching the formation of new closed flux surfaces. The corresponding Poincaré puncture plots are shown below each graph. At $t = 160$ two magnetic field lines (one red and one green) trace two new closed structures. The length of these lines is 3000 times the radius of the flux conserver. They can also be observed in the corresponding puncture plot, in green (the green line) and in black (the red line). Ten Alfvèn times later, the magnetic field lines beginning at the annulus concentrate around the magnetic axis, forming some nested closed flux surfaces surrounded by a chaotic region [Fig. 5 (b.2)]. In the final panel of Fig. 5 we can see that the nested closed flux surface occupy a larger volume around the magnetic axis, while the chaotic region becomes thinner. It is observed that these closed surfaces are nearly axisymmetric, while most of the $n = 1$ component remaining from the instability is asociated with the distortion of the central column. Fig. 6 shows the poloidal distribution of the magnetic energy density of the $n = 1$ mode, at $t = 250$. The $n = 1$ distortion localized in the central column remains until the end of the simulation.

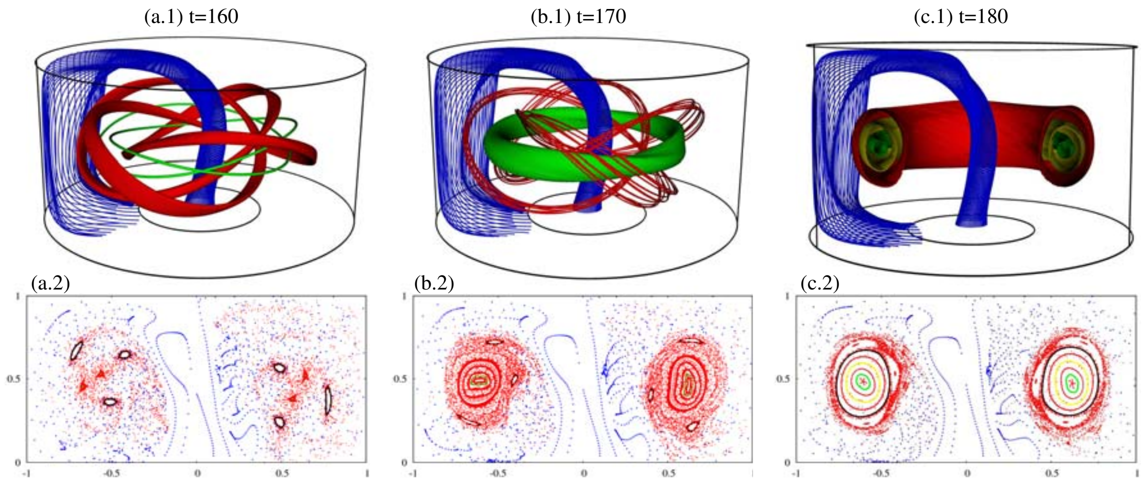

FIG. 5: (Color online) Formation of new closed flux surfaces. Blue field lines come from the electrode. Red, green and yellow lines begin at the annulus. These lines are also indicated in the corresponding puncture plot with the same color (except the red lines that are black in the puncture plots).

C. Dynamo effect

The MHD dynamo electric field parallel to the $n = 0$ component of the magnetic field is defined as $E_{d\|} = \langle \mathbf{v} \times \mathbf{b} \rangle \cdot \mathbf{B}_{n=0}/B_{n=0}$, where $\mathbf{v}$ and $\mathbf{b}$ are the non-axisymmetric fluctuations of the velocity and the magnetic field in the plasma, $\mathbf{B}_{n=0}$ is the $n = 0$ component of the magnetic field, and $\langle \cdot \rangle$ denotes toroidal averaging. Fig. 7 (a-f) shows colormap plots of the instantaneous $rE_{d\|}$ ($E_{d\|}$ times the radial coordinate r), for several times during the relaxation event, when the poloidal flux amplification takes place. The black contour separates dynamo ($E_{d\|} > 0$) from antidynamo ($E_{d\|} < 0$) regions. At $t = 100$ [Fig. 7(a)] a strong antidynamo localizes near the symmetry axis while a relatively weak dynamo appears in the closed flux region. As time advances, the dynamo region concentrates toward the magnetic axis and is surrounded by an antidynamo region. At $t = 140$ [Fig. 7(c)] there is a strong dynamo at the magnetic axis and a low value of $|rE_{d\|}|$ in the rest of the plasma. After this time the dynamo region fans out again. Finally, at $t = 170$ [Fig. 7(f)] a complex structure is observed, having weak dynamos and antidynamos in different regions (note the different scales in Fig.7).

Fig. 7(g) shows λ as a function of the poloidal flux, for the $n = 0$ component, at different

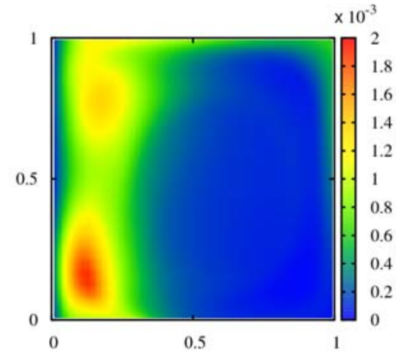

FIG. 6: (Color online) Magnetic energy density of the $n = 1$ mode at $t = 250$, in the poloidal plane.

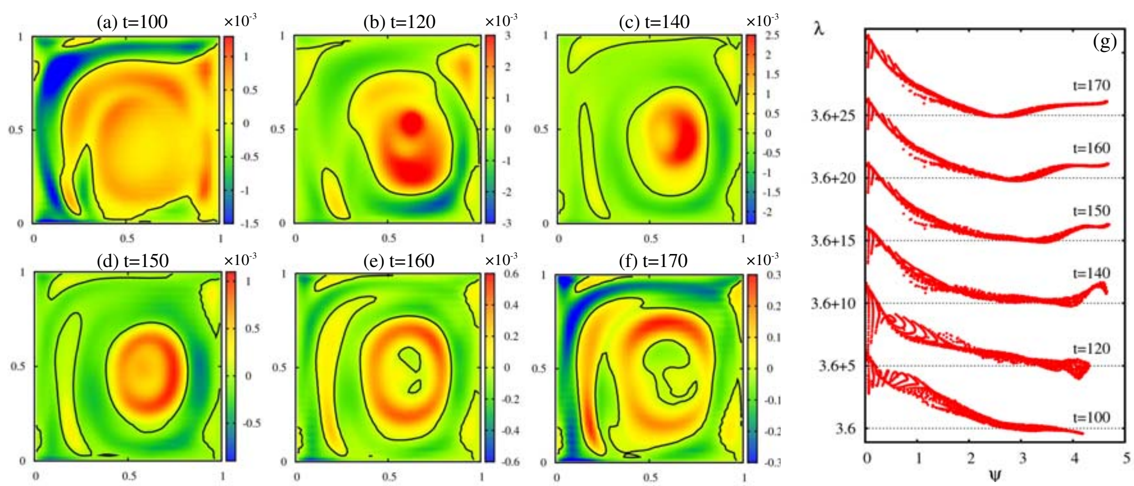

FIG. 7: (Color online) Instantaneous MHD dynamo electric field (multiplied by the radial coordinate) parallel to the axisymmetric component of the magnetic field (a-f). The black contour separates dynamo ($E_{d\|} > 0$) from antidynamo ($E_{d\|} < 0$) regions. $\lambda(\psi)$ profiles for several times during the relaxation period (g).

times during the relaxation period. This is done by plotting the pair of values $(\psi_{ij}, \lambda_{ij})$, obtained for each point of the poloidal grid, in the $\psi - \lambda$ space. In a perfectly axisymmetric equilibrium there should be only one value of λ for each value of ψ. However, when the flux surfaces are destroyed by the fluctuations this is no longer true. In agreement with the puncture plots, it is seen that at $t = 170$ the plot begins to collapse into a single line. We note that, during the relaxation, the dynamo region in the annulus evolves following roughly the contours of constant ψ. This behavior induces a wave-like motion in the $\lambda(\psi)$ profile, as observed in Fig. 7 (g).

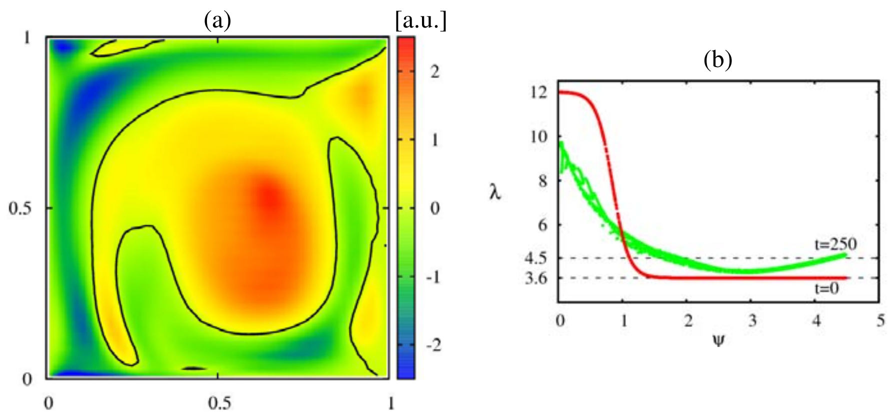

FIG. 8: (Color online) Temporal average of $E_{d\|}$ times the radial coordinate (a). Comparison between initial and final $\lambda(\psi)$ profiles (b).

The time average of the dynamo field (multiplied by r) computed over the full evolution is shown in Fig. 8 (a). We observe an antidynamo region near the geometric axis, and a dynamo region along the magnetic axis, with similar magnitudes. At the interface between the column and the annulus a structure with dynamo and antidynamo zones appears. The overall effect of the relaxation on the $\lambda(\psi)$ profile can be observed in Fig. 8 (b). The final profile is not flat, but the current has decreased in the open flux region ($\psi < 1$) and increased in the closed flux region ($\psi > 1$), as expected from the mean dynamo effect shown in Fig. 8 (a). Besides the evolution of $\lambda(\psi)$ caused by the dynamo action, observed in Fig. 7(g) (the dynamo takes place in the time interval $100 < t < 170$), the λ profile is smeared out by resistive diffusion, as noted when one compares the final profile shown in Fig. 8 (b) with the profile at $t = 170$ in Fig. 7 (g).

D. Evolution for an imposed λ_c

It is expected that during spheromak sustainment, λ_c will be determined mostly by the gun and λ_a will be maintained close to the stability boundary by the dynamo action of the kink. For a given value of λ_c, the stability of the central column to the kink mode is controlled by λ_a [12, 21]. In Fig. 9(a) we show the flux amplification factor as a function of time for $\lambda_c = 12$ and three values of λ_a. The three cases are kink unstable but the behavior of A_ψ changes significantly with relatively small changes in λ_a. When $\lambda_a = 3.8$ the flux

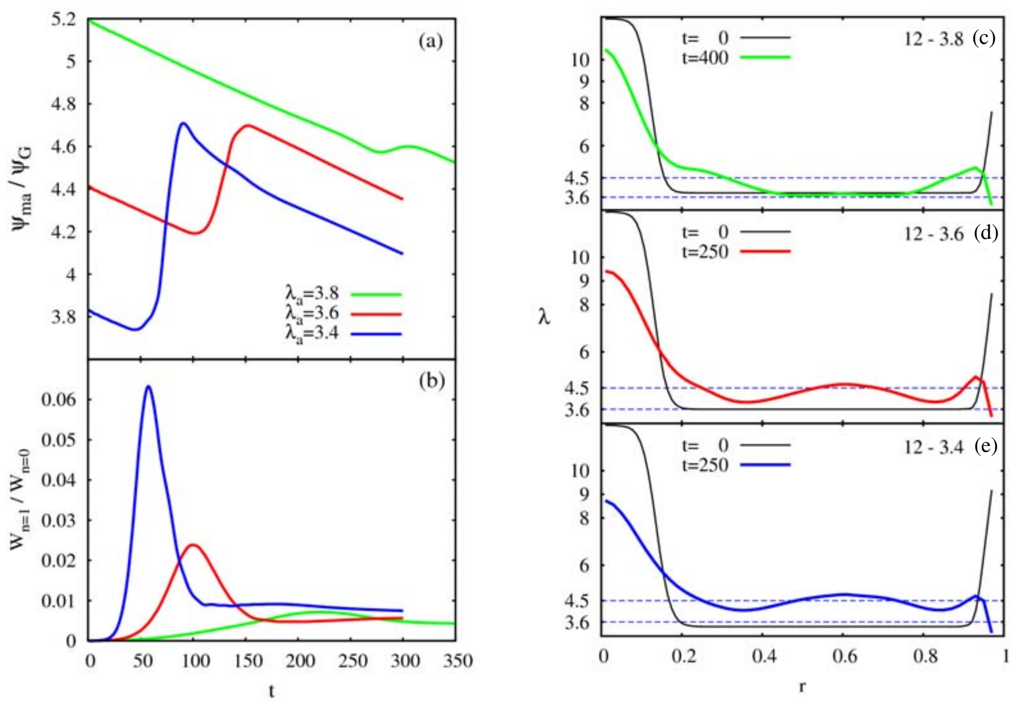

FIG. 9: (Color online) Evolution of the flux amplification factor (a) and ratio between the magnetic energies of the $n = 1$ and $n = 0$ modes (b), for three cases. Initial and final radial λ profiles of the $n = 0$ component, at $z = 0.5$ (c-e).

generated by the fluctuations is not enough to prevent A_ψ from decreasing rapidly. When $\lambda_a = 3.4$ (most unstable) a large flux amplification occurs and the final A_ψ is larger than the initial one. Finally, when $\lambda_a = 3.6$, A_ψ oscillates around 4.4 and we can conclude that the relaxation process produces enough poloidal flux amplification to compensate the resistive decay in the typical time scale of the instability. This is the reason why we study this case in more detail in the preceding sections.

In Fig. 9(b) we show the ratio between the magnetic energies of the $n = 1$ and $n = 0$ modes. This is an important parameter because it indicates the level of fluctuations that would be needed to sustain the configuration. In accordance with previous linear stability results, the growth rate of the instability increases when λ_a decreases [12]. Furthermore, the instability saturation level is higher for the more unstable cases. After saturation, the $n = 1$ fluctuation decreases down to a small but finite level. It was already mentioned that this feature was not observed in previous simulations without open flux, where a wide range of unstable initial conditions was studied [16], and it is associated to a helical distortion of the central column (Fig. 6). As observed in Fig. 5 (c), this remaining distortion does not prevent the formation of closed flux surfaces around the magnetic axis.

The radial λ profiles of the axisymmetric part of the solution are shown in Fig. 9 (c-e). We observe a very different behavior between the cases with $\lambda_a = 3.8$ and $\lambda_a = 3.6$. However, the more unstable situation produced by further decreasing λ_a down to 3.4, produces only minor changes in the final radial λ profile, when compared with the $\lambda_a = 3.6$ case. We conclude that a critical λ_a exists for the relaxation process, above which no significant redistribution of λ and no significant poloidal flux generation occur. This is the threshold around which we expect that the normal operation of a helicity-injected spheromak will take place. Note that this threshold lies in the unstable region of the stability map predicted by linear MHD stability computations [12]. The value of A_ψ at this threshold oscillates around 4.4, for the imposed $\lambda_c = 12$, which is consistent with experimental observations in SPHEX [22].

E. Effect of the resistivity

The level of fluctuations required to sustain the configuration is a crucial question in spheromak research. The evolution of the system around the threshold described in Sec. III D, involves a certain level of fluctuations (Fig. 9). It is of interest to study how this evolution and the associated level of fluctuations are modified by the Lundquist number. Fig. 10 shows the evolution of A_ψ and $W_{n=1}/W_{n=0}$ for three different values of S. The three cases have $\lambda_c = 12$ and different values of λ_a, indicated in the Figure. The new Lundquist numbers are obtained by setting $\tilde{\eta} = 5 \times 10^{-5}$ ($S \sim 800$) and $\tilde{\eta} = 1 \times 10^{-4}$ ($S \sim 400$). Besides a more rapid resistive decay, when S is decreased the saturation level of the $n = 1$

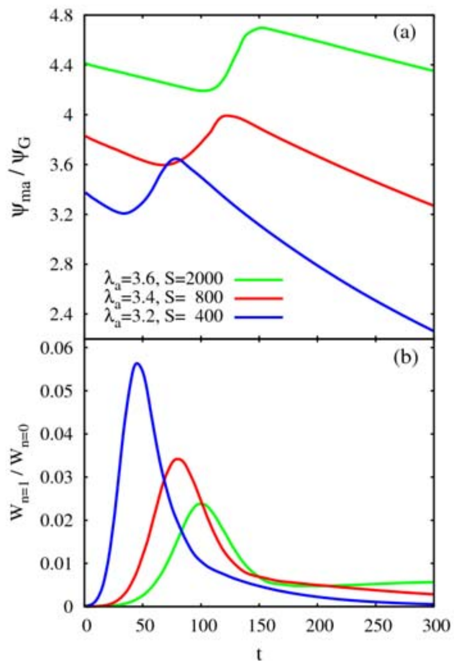

FIG. 10: (Color online) Evolution of the flux amplification factor (a) and the ratio between the magnetic energies of the $n = 1$ and $n = 0$ modes (b), for three values of S.

mode and the flux generation produced by a given unstable initial condition become lower (compare, for instance, the $\lambda_a = 3.4$ case with $S \sim 2000$ in Fig. 9, and with $S \sim 800$ in Fig. 10) [15, 16]. Thus, in Fig. 10, we compare three cases having different S and λ_a, in such a way that the initial configuration is more unstable when S is lower.

The evolutions shown in Fig. 10 indicate that when less resistivity is present, the fluctuations needed to sustain the configuration have a smaller saturation value and also a smaller growth rate. Therefore, we expect that, in a quasi steady situation, the fluctuations should not only decrease their amplitude but also become less frequent when S is increased. We also note that these results suggest that the value of S affects the maximum level of A_ψ that the system can achieve, for a given λ_c.

F. Evolution for different values of λ_c

While λ_c is externally imposed by the gun, the relaxation produced by the evolution of the kink instability will cause the system to oscillate around the threshold value of λ_a, below which significant current redistribution occurs and enough poloidal flux to sustain the configuration is generated. The search for this threshold is done for different λ_c values ($S \sim 2000$ in all cases). Fig. 11(a) shows A_ψ for four different pairs of values of λ_a and λ_c, very close to this threshold. The level of fluctuations resulting in these cases is shown in

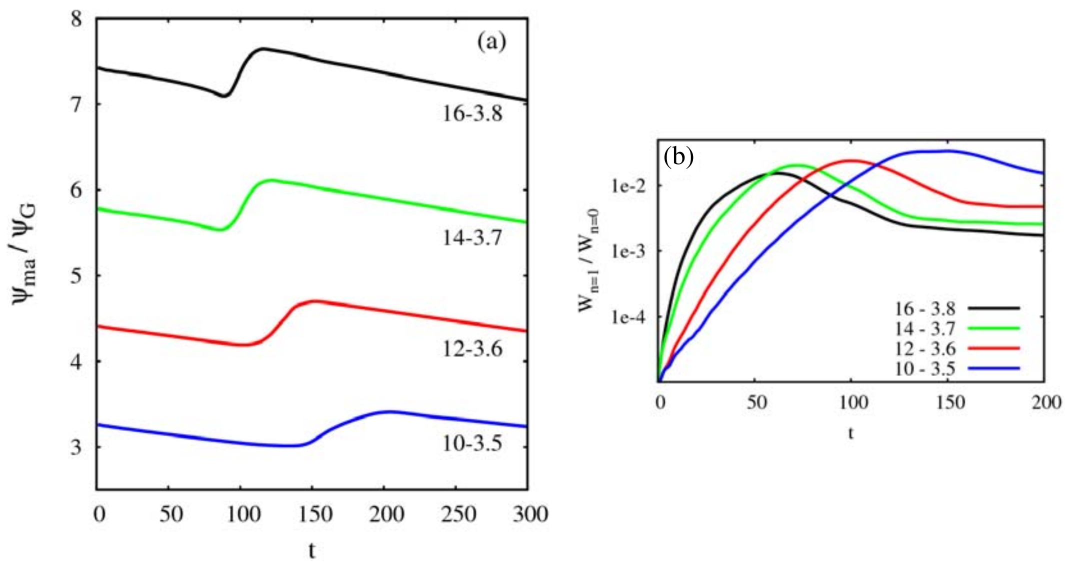

FIG. 11: (Color online) Flux amplification factor evolution for four cases with different initial values of (λ_c, λ_a) (a). Ratio between magnetic energies of the $n = 1$ and $n = 0$ modes (b).

Fig. 11(b). It is interesting to note that the smallest values of A_ψ require the largest relative values of the fluctuations (at saturation) and vice versa. Conversely, the growth rate of the $n = 1$ mode is lower for the cases with larger saturation values.

The results shown in Fig. 11(a) suggest that a sustained spheromak should have a larger A_ψ when the current imposed by the gun is increased (larger λ_c). However, as the value of λ_c is increased the dynamics of the relaxation becomes faster, as observed in Fig. 11 (b), so the system moves across regions with larger growth rates in the stability map [12, 21]. This implies that at higher λ_c values the relaxation redistributes the current in a shorter time scale. The current redistribution involves an increase of the toroidal current in the annulus and a decrease of mainly poloidal current in the central column (Fig. 8).

IV. CONCLUSIONS

We studied the non-linear evolution of several force-free equilibria inside a cylindrical flux conserver having open magnetic flux using the zero-β resistive MHD model. No external driving was applied but the initial conditions were chosen to simulate the conditions existing in a gun driven spheromak. These initial conditions have an almost stepwise current profile, with a high current density in the open flux region (λ_c) and a low current density in the closed flux region (λ_a). The pair of values (λ_c, λ_a) controls the stability of the configuration to the kink mode.

We computed the evolution of several equilibria having the same λ_c and different values of λ_a. A threshold value was found for λ_a above which the instability produces neither a significant λ redistribution nor enough flux amplification to sustain the configuration. The threshold for λ_a is 3.6 when $\lambda_c = 12$, and lies in the unstable region of the linear stability map [12]. Alternatively, one can think that the stability is controlled by the flux amplification factor since, when λ_c is fixed, there is a one to one correspondence between λ_a and A_ψ. In that sense, the computations presented in this work indicate that when A_ψ is higher than 4.4, the kink instability becomes too weak to sustain the configuration (for $S \sim 2000$, and $\lambda_c = 12$). This picture is very consistent with the experimental observation of a self-limiting current drive process which switches on if the annulus current falls too low and switches off if it is too high [11].

The case $\lambda_c = 12$ and $\lambda_a = 3.6$ was studied in detail because it is considered the most representative of the actual relaxation process during spheromak sustainment. We observed that the instability induces enough flux amplification to sustain the configuration, but the final profiles are far from a Taylor state with uniform λ. We also studied the behavior of the magnetic flux surfaces during this relaxation process. The central column of open flux develops a helical distortion which concentrates the return flux in a narrow toroidal region. This helical structure with a return column is very stable since it remains after the relaxation process has finished, leaving small but finite $n > 0$ components in the final configuration. This behavior was not observed in previous simulations without open flux [16, 20].

During the flux amplification, when the MHD dynamo is active, the initially closed flux surfaces are completely destroyed. After the end of the dynamo action, new nested surfaces surrounding the magnetic axis are rapidly formed. These new closed flux surfaces have an almost axisymmetric shape, while the $n > 0$ modes remaining in the energy spectrum at the end of the simulation are concentrated near the distorted central column.

We studied the evolution of the MHD dynamo electric field parallel to the $n = 0$ component of the magnetic field. A strong antidynamo ($E_{d\parallel} < 0$) is observed at the geometric axis. The dynamo region is initially distributed over the annulus, then it concentrates near the magnetic axis and it finally fans out again, ending with a complex structure of weak dynamo and antidynamo regions. The dynamo region advances approximately following surfaces of constant poloidal flux, thus producing a wave-like motion in the $\lambda(\psi)$ profile. This kind of evolution is probably responsible for the empirical fact that a tanh profile for λ does not fit the field data any better than a simple linear function of the flux [10]. The time averaged dynamo field (times the radial coordinate) exhibits an antidynamo region near the geometric axis, and a dynamo region around the magnetic axis with similar magnitudes. At the interface between the column and the annulus a structure with dynamo and antidynamo zones appears.

We studied the effect of the Lundquist number on the evolution. When more resistivity is present, the resistive decay is faster and the flux generation produced by a given unstable initial condition is smaller. Therefore, the system requires more unstable current profiles for sustainment, which leads to more frequent and larger fluctuations. As a result, the value of A_ψ around which the system oscillates, for a given λ_c, decreases with S.

The critical λ_a below which the instability evolution produces a significant current redistribution and enough flux amplification to sustain the configuration was explored for different λ_c values. The results clearly indicate that A_ψ increases with λ_c. This behavior was observed in experiments but only below a critical value of λ_c (~ 12.5) [22]. Above this limit the flux amplification of the configuration adotps a constant value. A possible explanation for this discrepancy can be drawn from dynamical considerations using the results presented here. In our simulations the external driving is introduced in the initial condition, so we can arbitrary set any current level in the open column. However, the current level of the central column is the result of a the competition between the external driving of the gun, which tends to increase this level, and the relaxation induced by the kink instability, which tends to decrease it. The results presented in this paper show that the dynamics of the relaxation becomes faster for higher λ_c values. Therefore, in order to sustain the configuration at a higher A_ψ, the external driving mechanism should be able to rise the current level of the open column more rapidly. With this consideration in mind, the critical value of λ_c above which A_ψ is constant could be due to a fast dynamics of the relaxation process that prevents the current in the open column from reaching higher values. Nevertheless, this conjeture remains to be tested, for instance, introducing a realistic model for the dynamics of the external driving process.

Acknowledgments

The authors gratefully acknowledge financial support from Universidad Nacional de Cuyo (Argentina), the Agencia Nacional de Promoción Científica y Tecnológica (ANPCyT). PLGM is supported by CONICET (Argentina).

---

[1] T. H. Jensen and M. S. Chu, Physics of Fluids **27**, 2881 (1984).

[2] T. R. Jarboe, Plasma Physics and Controlled Fusion **36**, 945 (1994).

[3] P. K. Browning, G. Cunningham, S. J. Gee, K. J. Gibson, A. Al-Karkhy, D. A. Kitson, R. Martin, and M. G. Rusbridge, Physical Review Letters **68**, 1718 (1992).

[4] E. B. Hooper, L. D. Pearlstein, and R. H. Bulmer, Nuclear Fusion **39**, 863 (1999).

[5] R. Raman, T. R. Jarboe, D. Mueller, M. J. Schaffer, R. Maqueda, B. A. Nelson, S. Sabbagh, M. Bell, R. Ewig, E. Fredrickson, et al., Plasma Physics and Controlled Fusion **43**, 305 (2001).

[6] T. R. Jarboe, P. Gu, V. A. Izzo, P. D. Jewell, K. J. McCollam, B. A. Nelson, R. Raman, A. J. Redd, P. E. Sieck, R. J. Smith, et al., Nuclear Fusion **41**, 679 (2001).

[7] F. Alladio, P. Costa, A. Mancuso, P. Micozzi, S. Papastergiou, and F. Rogier, Nuclear Fusion **46**, 613 (2006).

[8] J. B. Taylor, Reviews of Modern Physics **58**, 741 (1986).

[9] T. G. Cowling, Monthly Notices of the Royal Astronomical Society **94**, 768 (1934).

[10] D. M. Willett, P. K. Browning, S. Woodruff, and K. J. Gibson, Plasma Physics and Controlled Fusion **41**, 595 (1999).

[11] R. C. Duck, P. K. Browning, G. Cunningham, S. J. Gee, A. al-Karkhy, R. Martin, and M. G. Rusbridge, Plasma Physics and Controlled Fusion **39**, 715 (1997).

[12] D. P. Brennan, P. K. Browning, and R. A. M. van der Linden, Physics of Plasmas **9**, 3526 (2002).

[13] K. Katayama and M. Katsurai, Physics of Fluids **29**, 1939 (1986).

[14] C. R. Sovinec, J. M. Finn, and D. Del-Castillo-Negrete, Physics of Plasmas **8**, 475 (2001).

[15] V. A. Izzo and T. R. Jarboe, Physics of Plasmas **10**, 2903 (2003).

[16] P. L. García Martínez and R. Farengo, Physics of Plasmas **16**, 082507 (2009).

[17] G. Tóth, Astrophysical Letters & Communications **34**, 245 (1996), URL `www.phys.uu.nl/~toth/`.

[18] G. Tóth, Journal of Computational Physics **161**, 605 (2000).

[19] J. M. Finn and T. M. Antonsen, Comments Plasma Physics and Controlled Fusion **33**, 1139 (1985).

[20] P. L. García Martínez and R. Farengo, Journal of Physics Conference Series **166**, 012010 (2009).

[21] D. Brennan, P. K. Browning, R. A. M. van der Linden, A. W. Hood, and S. Woodruff, Physics of Plasmas **6**, 4248 (1999).

[22] M. G. Rusbridge, S. J. Gee, P. K. Browning, G. Cunningham, R. C. Duck, A. al-Karkhy, R. Martin, and J. W. Bradley, Plasma Physics and Controlled Fusion **39**, 683 (1997).